Time-Resolved PIV of high Re-number Combustion driven by Fractal Generated Turbulence

F. Hampp, K. H. H. Goh, M. A. Hadjipanayis, R. P. Lindstedt
Department of Mechanical Engineering
Imperial College, Exhibition Road
London SW7 2AZ, UK

1 Introduction

Turbulent flame acceleration is primarily governed by flow conditions (i.e. turbulence intensity) but also depends on mixture reactivity. The influence of obstructions in confined flame tubes, e.g. obstacle shape and blockage ratio (BR), have been the subject of previous studies featuring a wide range of mixtures containing a single fuel and air [1–10]. Increasing the BR gives rise to higher flame speeds due to higher turbulence generation, up to an optimal point where the increased BR results in (partial) flame quenching and momentum loss leading to flame deceleration. Consequently, mixtures are associated with an optimum BR to achieve their maximum flame speed [6]. Quantitative flow statistics is scarce due to the associated experimental challenges. However, flow and turbulent velocities obtained in flame tube featuring baffle-like obstacles have been reported by Lindstedt and Sakthitharan [11]. The mixture reactivity is dependent on fuel properties, equivalence ratio and initial conditions such as temperature and pressure. The effects of equivalence ratio and initial conditions have been investigated thoroughly [4, 6]. Studies concerning fuel mixtures are of increasing interest as fuel blending holds significant potential for further enhancement of the combustion process [12, 13]. For example, the addition of H_2 to CH_4 results in a lower effective activation energy and increased flame speed. The objective of the current study is to investigate flame acceleration in a stoichiometric mixture of 75% H_2/25% CH_4 with air and with initial turbulence generated by a cross fractal grid (CFG) followed by a solid 50% BR obstacle. The CFG is installed close to the ignition end to intensify turbulence in the unburned mixture ahead of the advancing flame leading to rapid flame acceleration. Geipel et al. [14] have shown that the substitution of conventional grids with CFGs results in a significantly increased turbulence intensity. The use of such grids has also been shown to result in multi-scale turbulence and enhanced flame wrinkling leading to an increase in the flame surface area and higher turbulent burning velocities [15]. The latter will lead to enhanced flame acceleration in the current context and such grids are thus used here to initiate high-speed turbulent deflagrations.

2 Experimental Setup

The experimental configuration, schematically shown in Fig. 1, features a flame tube with rectangular cross section of 0.072 m x 0.034 m and a length of 4.420 m. A number of CFGs were investigated, derived from the findings of Vassilicos and co-workers [16–18], and mounted at a distance of 115 mm from the ignition end. A solid obstacle, featuring a 50% BR, was mounted 402.5 mm from the same end capping the bottom half of the tube. The large length to hydraulic diameter (D_h) ratio (~ 96) of

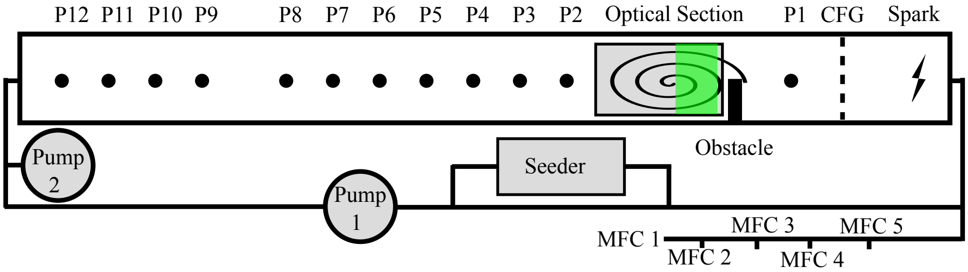

Figure 1: Schematic of the experimental setup with HS-PIV field of view indicated by the green rectangular; MFC - Mass Flow Controller.

Table 1: Port location (X) for installed pressure transducers (P) and ionisation (I) probes or both (PI).

Port	$P1$	$P2$	$P3$	$P4$	$P5$	$P6$	$P7$	$P8$	$P9$	$P10$	$P11$	$P12$
X [m]	0.27	0.90	1.14	1.37	1.60	1.84	2.08	2.31	3.30	3.60	3.90	4.20
Type	I	PI	I	PI	I	I	I	PI	PI	I	I	

the tube allows the investigation of flame-obstacle interactions without interference from acoustic waves reflected off the non-ignition end plate.

The basic instrumentation includes four piezo-electric pressure transducers (3xPCB-113B21 and 1xPCB-113A21; PCB Piezotronics Inc.) and twelve coaxial ionisation probes mounted along the length of the flame tube as specified in Table 1. The signals from the pressure transducers were interfaced to a PC via a signal conditioner (PCB 482C05; PCB Piezotronics Inc) and a 12-bit data acquisition card (PCI-6115; National Instruments) enabling a recording rate of 1 MHz. The ionisation probes used the same recording rate and served as flame detection devices providing complementary information on the propagation of the combustion wave. The probe design has been used extensively in the past and found to operate reliably [11,19,20]. The flame ions change the open-circuit resistance of the co-axial probes which were connected to an amplification circuit operated using 9 V batteries.

A high speed particle image velocimetry (HS-PIV) setup, controlled by LaVision Davis HS 8.0, was used to obtain flow velocities in the shear layer above and the recirculation zone behind the solid obstacle. The system, consisting of an Edgewave INNOSLAB Nd:YAG laser and a Photron Fastcam SA6, was timed and synchronised by an external LaVision HS controller. The camera was equipped with a 105 mm Nikkor camera lens (f5.6) with a mounted 3 nm narrow bandwidth filter for a wavelength 532 nm. The field of view was set to 76.0 mm $\times 63.3$ mm. The light sheet, indicated by the green rectangle in Fig. 1, featured a thickness of ~ 0.5 mm and was directed vertically from the top into the optical section of the flame tube. The silicone oil seeding, with an estimated droplet size < 1.5 μm based on the manufacturer specifications (Palas AGF 10) and previously used in an alternative geometry by [14], was introduced along with the flow through the inlet pipe. The recording rate was set to 10 kHz at a resolution of 576×480 pixels. The timing between the double laser pulses was found to be optimum at Δt $= 15$ μs. Subsequent to the data acquisition, dark image and background subtractions were performed to enhance the signal to noise ratio prior the calculation of conventional and time series PIV.

Before each experiment the flame tube was flushed with air and evacuated to a pressure below 0.5 kPa. A partial pressure method, using a static pressure transducer (UNIK 5000; GE Measurement & Control) [11] and controlled and monitored by a purpose written LabView interface, was applied to inject the required proportions achieving a stoichiometric fuel/air mixture consisting at $P_{init} = 45$ kPa. Mixture homogeneity was achieved by flow circulation using a diaphragm pump for 300 s corresponding

Table 2: Investigated CFG geometries where BR is the blockage ratio, t_{max} and t_{min} the maximum and minimum bar width, $t_r = t_{max}/t_{min}$, d_{hole} the diagonal of the cut-out and D the fractal dimension.

Grid No.	BR	t_{max} [mm]	t_{min} [mm]	t_r [mm]	d_{hole} [mm]	D
1	73.23%	4.0	1.50	2.67	3.20	2.0
2	63.53%	5.0	0.75	6.67	3.73	2.0
3	52.27%	4.0	0.50	8.0	4.27	2.0
4	43.64%	2.5	0.50	5.0	4.64	2.0

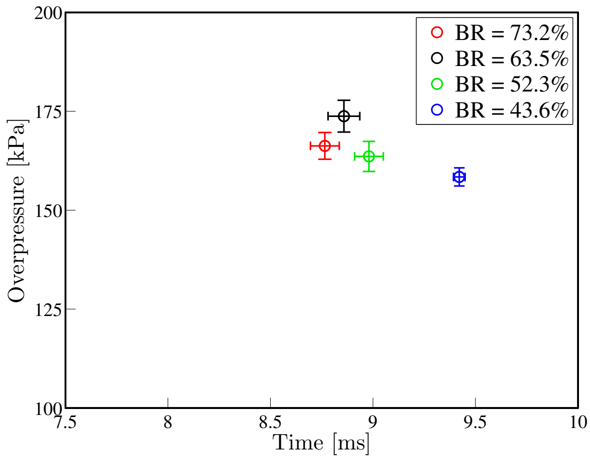

(a)

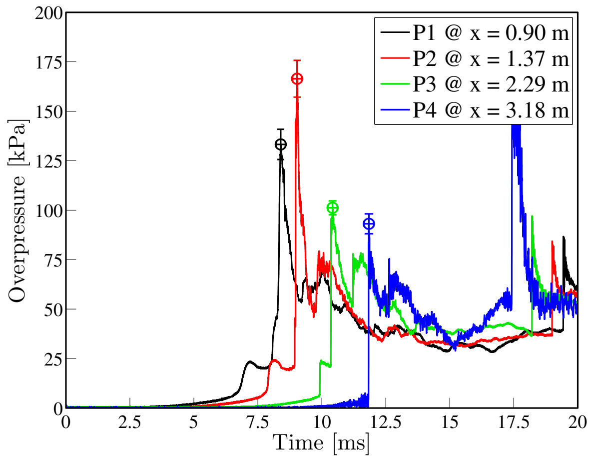

(b)

Figure 2: (a) The impact of the CFG blockage ratio on the maximum overpressure at Pressure transducer 2; (b) Over-pressure traces for four transducer locations using a CFG with BR= 52.3 % shown with the RMS of the peak pressure and pressure wave arrival time obtained from 11 experiments.

to 28 flame tube volumes. The mixture was left to settle for 120 s to achieve quiescent conditions before ignition. The ignition system consisted of a custom made control unit and spark plug - electrode arrangement (spark gap 10 mm) and an ignition coil. All data acquisition devices were triggered using TTL pulses ensuring the synchronisation of events.

3 Results and Discussion

The expansion of combustion products from the laminar flame kernel initiated by the spark drives the unreacted gas mixture ahead of flame front through the fractal grid. The passing of the flame through the CFG leads to substantial increase in flame surface area and consequently flame acceleration. As the flame subsequently approaches the solid obstacle, it first decelerates due to confinement followed by strong acceleration resulting from the enhanced turbulence levels in the recirculation zone behind the obstacle. A parametric study was carried out to investigate the impact of the CFG characteristics, i.e. BR and thickest to thinnest bar width ratio, on the initial turbulence generation and flame acceleration with the relevant grids listed in Table 2. It was found that the intensity of the initial flame acceleration is dependent on both parameters though only the BR variation is discussed here. The effect of the BR on the overpressure is shown in Fig. 2a. The CFG with the lowest BR resulted in an overpressure of 158 ± 2 kPa while the grid with BR of $\sim 63\%$ featured the highest overpressure of 174 ± 4 kPa, an increase of 10% for the tested mixture of 75% H_2 and 25% CH_4.

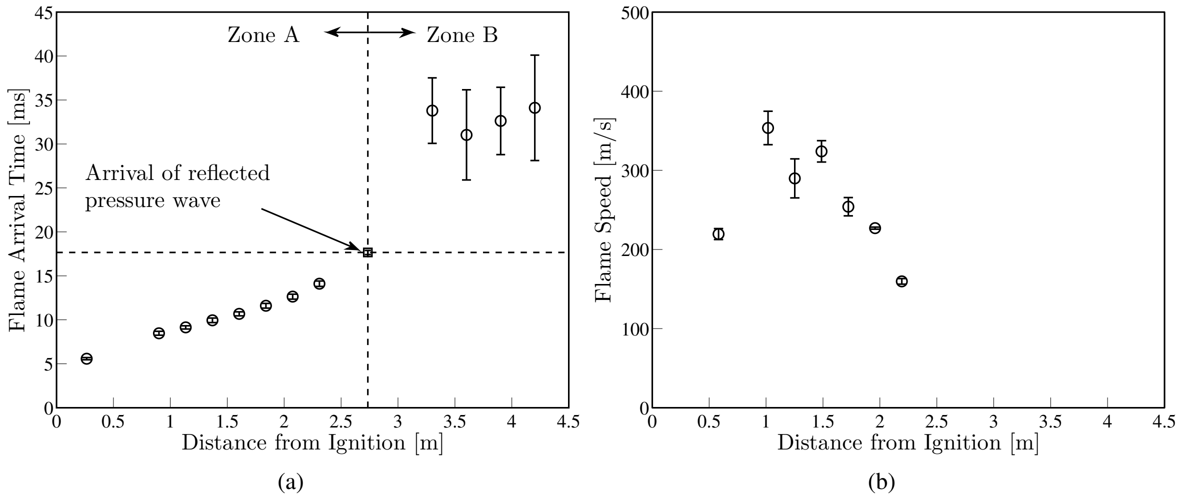

Figure 3: Flame arrival time and flame speed measured along the flame tube (a) Mean flame arrival time at each ionisation probe; (b) Average flame speed measured between two adjacent ionisation probes.

Grid 3 features a BR similar to the solid obstacle (BR $\approx 52\%$ vs. 50%) and was selected for subsequent experiments. Typical pressure traces can be seen in Fig. 2b. The detected uncertainty of peak pressure and timing was derived via the root mean square (RMS) from 11 runs. The average over-pressure at transducer two, situated just after recalculation zone, is $P_2 = 167 \pm 9$ kPa with an average pressure wave arrival times of $t_{P2} = 8.9 \pm 0.2$ ms. Considering the transient nature of the process being studied, the magnitude of the recorded uncertainties reflects the excellent reproducibility of the experiments and confirming the suitability of the experimental procedure. Given an initial pressure of $P_{init} = 45$ kPa the maximum relative over-pressure is $P_2/P_{init} = 3.71$. The moderate initial pressure built up, shown in Fig. 2b, results from the flame passing through the CFG. The flame front approach to the obstacle is followed by rapid acceleration resulting in an abrupt rise in pressure.

The mean flame arrival times, determined from the ionisation probes, are shown in Fig. 3 including the uncertainty obtained from the RMS. The dashed cross indicates an estimate where the pressure wave back reflection interacts with the flame front. The location and time of interaction is estimated linearly between port P8 and P9 ($x_{P8} = 2.31$ m, $x_{P9} = 3.30$ m). It is evident from the uncertainty magnitude that recorded data beyond this point, Zone B, are not reliable; hence are excluded from further analysis. However, the determined uncertainties in Zone A demonstrate the excellent reproducibility of the experiment. Furthermore, the flame speed is determined based on the distance between two adjacent probes and their respective recorded difference in flame arrival time with results depicted in Fig. 3b. The uncertainties were determined based on the flame arrival times. Due to the spacing and location of P1 and P2, the recorded flame speed at $x_{1.2}$ = 0.585 m represents an average value across the solid obstacle and is not the maximum occurring in this region. This indicates that using conventional flame detection devices it is difficult to resolve the local flame speed variations; hence the use of more advanced measuring techniques, e.g. HS-PIV, is essential in the recirculation zone. The highest flame speed is obtained between port P2 and P3 ($x_{2,3} = 1.02$ m). The flame arrival time at these ionisation probes corresponds to the pressure wave arrival time at pressure transducer two which records consistently the maximum over-pressure. Hence, the highest over-pressure is recorded at the point where the flame speed reaches its maximum.

HS-PIV at 10 kHz was used to determine the flow acceleration and velocities in the reactants. The technique also enables a qualitative interpretation of the flame surface structure as well as providing planar information on the flame arrival in the interrogation window. The use of silicone oil seeding (Dow Corning Xiameter PMX 200/50cS) leads to flame surface visualisation due to the evaporation of the droplets. The resulting iso-contour is located around 600 K and reasonably close to the $\sim$ 640 K iso-contour identified by Schlieren imaging as established by Weinberg [21]. The mean flame arrival time, based on the first occurrence in the optical section, was found to be $t_{fa} = 7.3 \pm 0.1$ ms. This shows excellent experimental reproducibility and is consistent with the flame arrival times obtained from the ionisation probe data. The extremely fragmented flame surface is shown in Fig. 4a by means of MIE scattering with determined PIV vectors superimposed. The flame enters the interrogation region in the upper part of the tube, dividing the mixture into burnt (top) and unburnt (bottom) regions, and subsequently circulates back at the bottom into the interrogation region against the main flow direction. Also shown in Fig. 4a are examples of analysis windows (A, B, and C) used to compute the time evolution of the mean velocity magnitude and velocity components based on Eq. (1) where I and J are dimensions of the analysis windows in x and y direction respectively. The locations of the analysis windows A, B, and C were chosen to represent the velocities in the free flow, shear layer and recirculation zone respectively. Vectors with nil value have been excluded.

$$\begin{aligned}
\overline{u} &= \frac{\sum_r^R \sum_i^I \sum_j^J u_{r,i,j}}{R \times I \times J} \quad ; \quad \overline{v} = \frac{\sum_r^R \sum_i^I \sum_j^J v_{r,i,j}}{R \times I \times J} \\
|\overline{u}| &= \frac{\sum_r^R \sum_i^I \sum_j^J \sqrt{(u_{r,i,j}^2 + v_{r,i,j}^2)}}{R \times I \times J} \\
|\overline{u}|_{rms} &= \frac{\sqrt{\sum_r^R ((\sqrt{(u_r^2 + v_r^2)} - |\overline{u}|)^2)}}{R}
\end{aligned} \tag{1}$$

The determined mean horizontal ($\overline{u}$) and vertical ($\overline{v}$) velocity components, as well as the velocity magnitude $|\overline{u}|$ and its RMS value $|\overline{u}|_{rms}$, were obtained from the 11 runs (R) where HS-PIV was carried out and are depicted in Fig. 4b. The approach serves as an illustration of data processing. However, the best way to compare data with time-dependent calculation methods, such as LES, is subject to debate. The velocities reported here correspond to the mean flow of reactants just after the flame passes the obstacle. The relatively large uncertainties obtained between $6 - 7$ ms result partly from the slight differences in flame arrival times at the obstacle. It is evident that the mean velocities in the free flow (frame A) are significantly higher than in the shear layer (frame B). The sharp rise in negative $\overline{v}$ in frame C after $\sim$5 ms is indicative of the temporal development of the recirculation eddy. The subsequent increase towards positive values at times > 6.2 ms indicates the downstream movement (away from the from obstacle) of the eddy. The mean local maximum velocity is $\overline{u}_{max} = 432$ m/s with the absolute maximum $u_{max} = 453$ m/s. The maximum velocities coincide approximately with the flame arrival in the optical section ($t_{fa} \simeq 7.3$ ms) and are subject to large stochastic variations due to the intensity of the turbulent explosion. Accordingly, the time axis in Fig. 4b is truncated before this event. Using $\overline{u}_{max}$ and the hydraulic diameter of the tube, a Reynolds number around $5.6 \cdot 10^5$ at $P_{init} = 45$ kPa is obtained. Lindstedt and Sakthitharan [11] determined turbulence intensities of $10 - 20\%$ in an identical device without the CFG allowing an estimate of the turbulent Reynolds number as $Re_t \approx 1.0 \cdot 10^5$.

4 Conclusion

The transient combustion of hydrogen/methane mixtures at Reynolds numbers up to $5.6 \cdot 10^5$ has been studied using high speed PIV (HS-PIV) at 10 kHz with supplementary data obtained using ionisation probes and pressure transducers. The use of cross fractal grids (CFGs) to initiate the transition to turbulent flame propagation results in estimated turbulent Reynolds numbers of approximately 10^5 and heavily fragmented flames. The measurements provide a comprehensive quantification of the flame acceleration process with the highly fragmented flame structure verified by means of MIE scattering

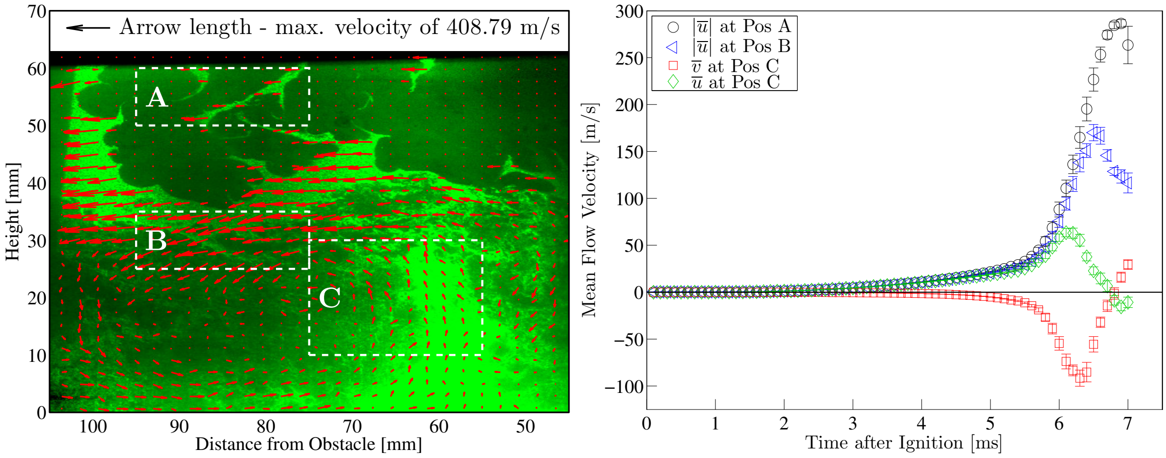

(a) (b)

Figure 4: Flow velocity in the reactants: (a) Visualisation of the flame surface by means of MIE scattering with determined PIV vectors superimposed at 7.4 ms after ignition; (b) Mean reactant velocity in analysis windows (A, B, C).

images. The use of CFGs entails the advantage of multi-scale turbulence generation with the intensity level depending on the grid characteristics. It was shown that the BR exhibits a significant impact on the flame acceleration process and an optimised configuration was obtained. The latter featured a CFG with $\sim 52\%$ BR which was used for a more detailed flame characterisation yielding a maximum relative over-pressure of $P_{over}/P_{init} \approx 4$ and a local maximum flame speed of $U_f > 350$ m/s. Uncertainty analysis on pressure, ionisation probe and HS-PIV data showed excellent repeatability and verifies the experimental procedure. Time resolved data of the over-pressure traces allowed the separate identification of pressure build up due to the flame acceleration initiated by the CFG and obstacle. In combination with the flame arrival time data, it further quantified the link between flow velocities, flame speed and the resulting overpressure. The unreacted gas flow velocities were obtained by means of HS-PIV in the recirculation zone behind the obstacle showing the displacement effect of the fresh gas by the hot combustion products. It is expected that the data sets produced will enable a multi-parameter (e.g. flow velocities and over-pressures) validation of calculation methods aimed at representing the temporal evolution of such high speed flows and thereby support the development of improved tools for the quantitative risk assessment of explosion hazards.

5 Acknowledgements

The authors would like to acknowledge the support of the ONR under Grant N62909-12-1-7127 and AFOSR and EOARD under Grant FA8655-13-1-3024. The authors wish to thank Dr Gabriel Roy, Dr Chiping Li and Dr Gregg Abate for encouraging the work. The US Government is authorized to reproduce and distribute reprints for Governmental purpose notwithstanding any copyright notation thereon.

References

[1] Johansen C.T., Ciccarelli G. (2009). Visualization of the unburned gas flow field ahead of an accelerating flame in an obstructed square channel. Combust. Flame 156 (2): 405-416.

[2] Lee J.H.S., Knystautas R., Freiman A. (1984). High speed turbulent deflagrations and transition to detonation in H_2-air mixtures. Combust. Flame 56 (2): 227-239.

[3] Silvestrini M., Genova B., Parisi G., Trujillo F.J.L. (2008). Flame acceleration and DDT run-up distance for smooth and obstacles filled tubes. J. Loss Prev. in the Process Industries 21 (5): 555-562.

[4] Ciccarelli G., Dorofeev S. (2008). Flame acceleration and transition to detonation in ducts. Prog. Energy Combust. Sci. 34 (4): 499-550

[5] Alekseev V.I., Kuznetsov M.S., Yankin Y.G., Dorofeev S.B. (2001). Experimental study of flame acceleration and the deflagration-to-detonation transition under conditions of transverse venting. J. Loss Prev. in the Process Industries 14 (6), 591-596.

[6] Beauvais R., Mayinger F., Strube G. (1994). Turbulent flame acceleration-mechanisms and significance for safety considerations. Int. J. Hydrogen Energy 19 (8): 701-708.

[7] Chan C.K., Loesel Sitar J.L., Beauvais R., Mayinger F. (1996). Modeling maximum flame speeds. Nuclear Engineering and Design 166 (3): 463-469.

[8] Lee J.H.S, Knystautas R., Chan C.K. (1985). Turbulent flame propagation in obstacle-filled tubes. Proc. Combust. Inst. 20 (1): 1663-1672.

[9] Teodorczyk A. (2008). Scale effects on hydrogen-air fast deflagrations and detonations in small obstructed channels. J. Loss Prev. in the Process Industries 21 (2): 147-153.

[10] Kratzel T., Burkhardt A., Eichert H., Fischer M. (1996). Instationary highly turbulent hydrogen tube combustion processes in obstacle areas. Int. J. Hydrogen Energy 21 (1): 45-52.

[11] Lindstedt R.P., Sakthitharan V. (1998). Time Resolved Velocity and Turbulence Measurements in Turbulent Gaseous Explosions. Combust. Flame 114 (3-4): 469-483.

[12] Lieuwen T., McDonell V., Petersen E, Santavicca D. (2008). Fuel Flexibility Influences on Premixed Combustor Blowout, Flashback, Autoignition,and Stability. J. Eng. Gas Turbines Power 130 (1): (011506).

[13] Williams T.C., Shaddix C.R., Schefer R.W. (2007). Effect of Syngas Composition and CO2-Diluted Oxygen on Performance of a Premixed Swirl-Stabilized Combustor. Combust. Sci.Technol. 180 (1): 64-88.

[14] Geipel P., Goh K.H.H., Lindstedt R.P. (2010). Fractal-Generated Turbulence in Opposed Jet Flows. Flow Turbul. Combust. 85: 397-419.

[15] Goh, K.H.H, Geipel, P., Hampp, F., Lindstedt, R.P. (2013) Flames in fractal grid generated turbulence, Special Issue of Fluid Dynamics Research on Turbulent Flows Generated/Designed in Multiscale/Fractal Ways, Accepted for publication.

[16] Vassilicos J.C., Hunt J.C.R. (1991). Fractal dimensions and spectra of interfaces with application to turbulence. Proc. R. Soc. Lond. A 435: 505-534.

[17] Seoud R.E., Vassilicos J.C. (2007). Dissipation and decay of fractal-generated turbulence. Phys. Fluids 19: (105108).

[18] Hurst D., Vassilicos J.C. (2007). Scalings and decay of fractal-generated turbulence. Phys. Fluids 19: (035103).

[19] Lindstedt R.P., Michels H.J. (1988). Deflagration to detonation transition in mixtures of alkane LNG/LPG constituents with O_2/N_2. Combust. Flame 72 (1): 63-72.

[20] Lindstedt R.P., Michels H.J. (1989). Deflagration to detonation transitions and strong deflagrations in alkane and alkene air mixtures. Combust. Flame 76 (2): 169-181.

[21] Weinberg F.J. (1956). The Shadowgraph of a Flat Flame. Proc. R. Soc. Lond. A 235: 510-517.